Saudi Journal of Biological Sciences 27 (2020) 2638–2644

Contents lists available at ScienceDirect

Saudi Journal of Biological Sciences

journal homepage: www.sciencedirect.com

Original article

Cryogel biocomposite containing chitosan-gelatin/cerium–zinc doped hydroxyapatite for bone tissue engineering

Shiqing Wu [a,*], Shengzhong Ma [a], Cheng Zhang [a], Guangqing Cao [a], Dongjin Wu [a], Chunzheng Gao [a], Sivalingam Lakshmanan [b,*]

[a] Department of Spinal Surgery, The Second Hospital of Shandong University, No.247 Beiyuan Road, Tianqiao District, Jinan City, Shandong Province 250033, China
[b] Department of Chemistry, BIHER, Bharath University, Chennai 600 073, India

ARTICLE INFO

Article history:
Received 13 April 2020
Revised 21 May 2020
Accepted 27 May 2020
Available online 1 June 2020

Keywords:
Antibacterial activity
Cryogel
Biocomposite
Bone
Chitosan
Hydroxyapatite

ABSTRACT

The present examination includes manufacture and portrayal of cryogel bio-composite implants containing chitosan-gelatin (CS-GT), cerium–zinc doped hydroxyapatite (CS-GT/Ce-Zn-HA) by cryogelation technique. The prepared cryogel biocomposites (CS-GT/HA and CS-GT/Ce-Zn-HA) were described by scanning electron microscope (SEM) and X-Ray diffraction (XRD) contemplates. The expansion of Ce-Zn in the CS-GT implants essentially expanded growing, diminished swelling, expanded protein sorption, and expanded bactericidal movement. The CS-GT/Ce-Zn-HA biocomposite had non-toxic towards rodent osteoblast cells. So the created CS-GT/Ce-Zn-HA biocomposite has favorable and potential applications over the CS-GT/HA platforms for bone tissue engineering.

1. Introduction

Bone tissue engineering (BTE) is one of the key alternative treatment methods for regenerating bone tissue (Liu and Ma, 2004; Kumar Meena et al., 2020). In the classical tissue-building approach, solid cells that are typically confined from the patient's tissue are seeded in implants arranged from polymers, legitimately or in the wake of growing in cell incubation, and this development is then embedded into the surrendered zone (Ng et al., 2017; Carrabba and Madeddu, 2018). Hydroxyapatite (HA) is for the most part utilized in bone tissue engineering because of its comparable crystallography with that of common bony mineral which is broadly chosen for bony embed related applications (Huang et al., 2019; Kumar et al., 2019). HA are having not many issues, for example, poor bactericidal characteristics and fragility which makes it unsatisfactory for orthopedic applications (Yavarpanah et al., 2019; Stevanović et al., 2019). This downside prompts the danger of bacterial adherence to implants covered with pristine HA (Arcos and Vallet-Regí, 2020). Normally happening to follow components in bones (Magnesium, Zinc, Manganese, Strontium, Ag, Cerium, Copper) could be utilized as doping in HA to forestall microbial infections (Arcos and Vallet-Regí, 2020; Anastasiou et al., 2019). Zn is one of the significant follows components present in normal bone. Zinc is basic for different natural capacities, for example, compound cofactors and biomineralization, DNA replication and bone development (Ma and Yamaguchi, 2001; Yamaguchi 2010). Consolidating zinc into HA improves bioactivity and shows great outcomes *in vivo* osteoblast cell line considers. The moderate take-up and arrival of zinc particles help in quickening bony development and arrangement around the inserts (Yang et al., 2012; Huang et al., 2015). Cerium (Ce) helps in initiating and improving the ligand authoritative and cell grip of integrins (Naganuma and Traversa, 2014). Integrins have a place with the gathering called trans-membrane receptors which helps in cell bond of the extracellular network. Ligand restricting aides in actuating the integrins and permits moment reactions at the outside of the cell (Bachmann et al., 2019; Hintermann and Christen, 2019)

Then again, cell-relocating and development actuating operators are fused into the implants, which are embedded legitimately into the imperfection territory. Perfect implants ought to be permeable, degradable and non-toxic, and its mechanical characteris-

* Corresponding authors.
E-mail address: orthdoctor@sina.com (S. Lakshmanan).
Peer review under responsibility of King Saud University.

Production and hosting by Elsevier

https://doi.org/10.1016/j.sjbs.2020.05.045
1319-562X/

tic ought to be like those of the host tissue (Parai and Bandyopadhyay-Ghosh, 2019). To get ready permeable grids to be utilized as tissue-designing implants, various techniques, for example, electrospinning, lyophilize, cryogelation and gas frothing, and so on., have been accounted for (Milazzo et al., 2019; Nikolova and Chavali, 2019). Normally determined or engineered polymers have been utilized to fabricate implants that give formats to fresh tissue recovery while the implant is progressively assimilated.

Cryogelation is a straightforward and powerful strategy for delivering porous implants having controlled pore size (Tripathi and Melo, 2019). This strategy permits successful command over the pore volume utilizing ice gems as formats for creating a porous implant structure. As the lattices are permitted to crosslink at below zero temperatures, the ice precious stones framed inside the implants go about as porogen and result in interconnected pores inside the gelled grid in the wake of defrosting. Considering the different characteristics of cryogels, for example, their interconnected pores, versatility, mechanical steadiness, reversibility, and growing capacity, it would be appropriate for tissue recovery (Saini et al., 2019; Liu et al., 2019).

The point of this examination was to fabricate degradable chitosan-gelatin/cerium–zinc doped hydroxyapatite -based biocomposite with interconnected pores to be utilized as implants in tissue recovery, essentially for bony. Biocomposites were integrated and their phase structure, swelling proportion, debasement profile, mechanical characteristic, and surface structure were illustrated. *In vitro* cell feasibility tests were evaluated to show the biocompatibility of the cryogels and biocomposite. At long last, in vitro biocompatibility assay were led to show the capability of the biocomposite for future bone tissue-designing applications.

2. Materials and methods

2.1. Preparation of Ce-Zn-HA nanoparticles

For the fabrication of Ce-Zn-HA, the technique was equivalent to the past (Dasgupta et al., 2010). A watery arrangement of 0.9 M calcium chloride, 0.05 M zinc chloride, 0.05 cerium chloride and 0.6 M diammonium hydrogen phosphate were utilized. The above blend was then mixed for 5 h and the pH was continually balanced and kept up at 10 during the response of the amalgamation. All the accelerates were washed thrice and afterward set in an oven and warmed at 100 °C for 24 h to acquire the dried nanoparticles.

2.2. Preparation of cryogel biocomposite

For the Fabrication of CS-GT cryogel, the methodology was equivalent to the past (Kemençe and Bölgen, 2017). The entire chemical was purchase from sigma-Aldrich trading Co., Ltd (Shanghai china). The cryogel biocomposite was prepared as follows: CS-GT cryogel and Ce-Zn-HA nanoparticles particles were added to DD water and mixed at 37 °C for 10 h to shape a slurry with the last grouping of 5% w/w CS-GT cryogel and 15% w/w Ce-Zn-HA nanoparticles. The slurry was crosslinked utilizing glutaraldehyde arrangement at 5 °C for 1 h, at −10 ^{0}C for one day, and thusly freeze-dried for 2 days.

2.3. Cryogel biocomposite characterization

The scanning electron microscopy images (SEM JEOL JSM-5410LV) and X-ray diffraction (XRD Siemens D5005) of the different biocomposites were investigated.

2.4. Swelling test

Equivalent measures of CS-GT/HA and CS-GT/Ce-Zn-HA implants were taken and their dry loads were noted. The biocomposites were then inundated in 250 μl of arrangement for 24 h and 48 h at RT. The biocomposites were expelled and smudged on channel paper to evacuate consumed water and wet loads of the frameworks were noted. The trial was acted in triplicates.

2.5. Biodegradation study

The biocomposites were similarly gauged and the dry loads of the biocomposites were noted. They were then submerged in media containing lysozyme at a fixation like that of flowing degrees of blood. Brooding was done at various time interims as follows: 1–3 days at RT. Toward the finish of the hatching period, the biocomposites were washed with DD water to expel any particles adsorbed on the surfaces and blotch dried utilizing channel paper. The investigation was done in triplicates.

2.6. Protein adsorption assay

The biocomposites were similarly gauged and pre-wetting was done in a hermetically sealed compartment to expel air rises from the framework. The biocomposites were then brooded for 24 and 48 h in the dulbecco's modified eagle medium containing fetal bovine serum at RT. After brooding, the biocomposites were expelled, smudge dried and tenderly washed with phosphate-buffered saline thrice to evacuate any free and inexactly adsorbed proteins from the biocomposites. The proteins adsorbed onto the frameworks were then eluted by hatching the platforms in SDS for one hour with persistent tumult. This progression was rehashed for thrice to acquire total elution of the proteins adsorbed onto the platforms. The examples were then pooled together. The aggregate sums of adsorbed proteins were resolved to utilizing Lowry's technique. The analysis was done in triplicates.

2.7. Antibacterial activity

The antibacterial characteristics were controlled by the zone of restraint test utilizing *S. aureus* and *E. coli*. The overnight incubation was readied. 50 μl of the overnight microbial seeding (1×10^4 CFU/ml) was stretch onto agar plates; 0.5 mg of the platform was set on the plates in triplicates, trailed by brooding for one day at RT.

2.8. Osteogenesis study

Thereafter, the lysates acquired were taken to another well plate and estimated by the pack guidance. Mineralization was assessed by measuring the development of calcium phosphate ARS. At days 3 and 7, all cell substrates were attached in paraformaldehyde for 60 min and washed multiple times with phosphate-buffered saline, trailed by recoloring with ARS for 1 h; the cell substrates were in this manner flushed with adequate DD water. The action of alkaline phosphatase was estimated utilizing an ALP examine unit at day 1, 3 and 7 of osteogenic enlistment. At each time point, the solution was disposed of and all osteoblast cell substrates were flushed with phosphate-buffered saline and lysed with Triton arrangement at RT for 1 h. Finally, the supernatant was estimated at 562 nm utilizing a spectrophotometer.

2.9. Cell cytotoxicity and proliferation

Cell cytotoxicity and multiplication were estimated utilizing cell checking pack-8 reagent (CCK-8). Quickly, at the different time

focuses including 24 h, 48 h, and 72 h, the bone marrow stromal cells seeded platforms and layers were hatched in CCK-8 arrangement at RT in a hatchery with CO_2 for 60 min. Subsequently, the supernatant got was taken to another well plate and estimated at 450 nm utilizing a microplate peruser.

2.10. Statistical analysis

The obtained data are reported as mean ± standard deviation (SD). The one-way analysis of variance (ANOVA) with the post hoc Tukey's method was performed to exam the statistical analysis.

3. Results and discussion

3.1. Phase and morphological analysis

The X-ray diffraction of CS-GT/HA and CS-GT/Ce-Zn-HA cryogel biocomposite has appeared in Fig. 1 A. The XRD of CS-GT/HA cryogel biocomposite the diffraction tops at 33°, 31°, 29°, and 20° which relate to the 2 theta estimations of CS-GT and HA, individually. The X-ray diffraction of CS-GT/Ce-Zn-HA cryogel biocomposite indicated three planes at 36°, 34°, and 31° comparing to the planes of Zn, and tops at 74°, 49°, and 43° relating to (2 2 0), (2 0 0) and (1 1 1) planes of cerium which is in concurrence with the JCPDS no. 09-0432 (Ren et al., 2009; Phatai et al., 2018). Moreover, the crystalline planes of HA in the cryogel biocomposite showed that the expansion of Ce-Zn compound nanoparticles didn't change the crystalline idea of CS-GT/HA cryogel biocomposite.

The SEM micrographs uncovered the pressed and porous surface of CS-GT/HA cryogel biocomposite (Fig. 1B) while a permeable and harsh surface if there should arise an occurrence of CS-GT/Ce-Zn-HA cryogel biocomposite (Fig. 1B) along these lines demonstrating that the mixing of Ce-Zn with HA positively changed the surface morphology. The permeable morphology of cryogel biocomposite builds the surface zone bringing about high supplement conveyance, better protein adsorption, neovascularisation and relocation to the site of tissue recovery (Ansari 2019; Zhu et al., 2020). Also, the surface roughness improved the integrin-subordinate connection of bony cells. Consequently, CS-GT/Ce-Zn-HA satisfies the pre-necessities of a perfect bone simple in a better manner in examination than CS-GT/HA cryogel biocomposite.

3.2. Swelling test

To decide the water maintenance or take-up property of the implants which is one of the significant characteristics required for implants to be utilized in bony tissue building, the biocomposites were oppressed for growing examinations as portrayed in Section 3.1. The swelling test showed that toward the finish of the 24 h hatching period, there was no noteworthy contrast in the growing proportion among the CS-GT/HA and CS-GT/Ce-Zn-HA frameworks. At the point when the brooding time frame was saved for 48 h, there was essentially expanded growing proportion by the CS-GT/Ce-Zn-HA, for example, CS-GT/Ce-Zn-HA held more water than their underlying weight contrasted and CS-GT/HA cryogel biocomposite (Fig. 2). This is recommended that the swelling capacity would guide to increment in the pore volume and invasion of bone cells easily bringing about better bony tissue ingrowths (Asadpour et al., 2019).

3.3. Biodegradation study

The chains of N-acetyl glucosamine connected by glycosidic bonds are the dynamic destinations for an entry point and chain

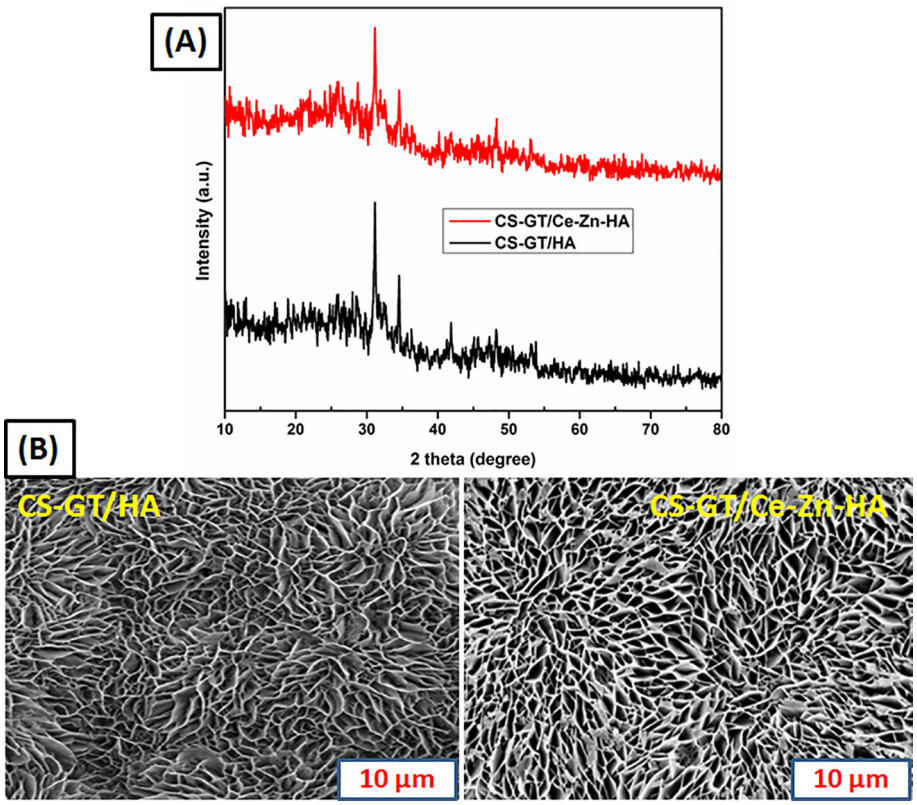

Fig. 1. (A) XRD and (B) SEM images of prepared cryogel biocomposites.

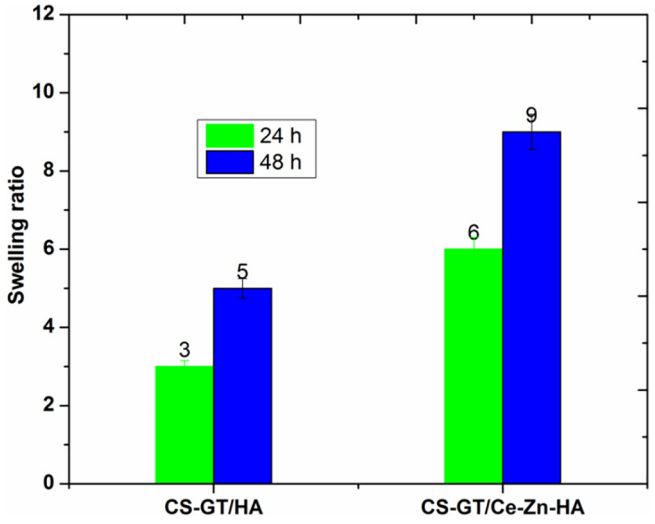

Fig. 2. Swelling test prepared cryogel biocomposites were carried out by submerging them in phosphate-buffered saline medium for 24 and 48 h at room temperature.

hydrolysis by lysosyme (Yadav et al., 2019). The biodegradation prompts the arrival of amino sugars, which can be fused into glycosaminoglycans and glycoprotein metabolic pathways, or discharged. Since the pace of debasement of the platforms is probably going to be basic for the discharge of the bioactive fixings as well as for giving the mechanical quality, the ex vitro biodegradation analyze was completed (Fig. 3). The debasement paces of CS-GT/HA and CS-GT/Ce-Zn-HA platforms were resolved at 24 h and 48 h. The debasement paces of the CS-GT/Ce-Zn-HA frameworks were negligible contrasted with CS-GT/HA platforms at 1–3 days (Fig. 3).

3.4. Protein adsorption study

The measures of proteins adsorbed onto the cryogel biocomposite platforms at 24 and 48 h were controlled by Lowry's technique. Toward the finish of the 24 h time span, there was no huge change in the measures of protein adsorbed between the CS-GT/HA and CS-GT/Ce-Zn-HA frameworks. At the point when the hatching time cryogel biocomposite was expanded, for example, 48 h, the measures of proteins adsorbed onto the CS-GT/Ce-Zn-HA framework were essentially expanded when contrasted and the CS-GT/HA cryogel biocomposite (Fig. 4). This could be because of the way that the expansion of Ce–Zn-HA nanoparticles would have expanded the surface region and hydrophilicity of the platforms, and thus more proteins were adsorbed. Expanded protein adsorption of the cryogel biocomposite would prompt have better cell network communication, attachment and spreading on the cryogel biocomposite (Dave and Gomes, 2019).

3.5. Antibacterial activity

This examination was planned for creating cryogel with the consolidation of Ce–Zn-HA nanoparticles which have characteristic antibacterial movement. The expansion of Ce–Zn-HA in the CS-GT cryogel for the antibacterial movement was checked by a zone of restraint utilizing *S. aureus and E. coli* bacterial strains (Fig. 5). The zone restraint for the CS-GT/Ce-Zn-HA was seen as 12.5 ± 4 m m and 22.5 ± 3 mm against *S. aureus* and *E. coli*, individually. While the zone of a hindrance for the CS-GT/HA was similarly lower as 8. 2 ± 2 mm and 3.8 ± 4 mm against *E. coli* and *S. aureus*, separately.

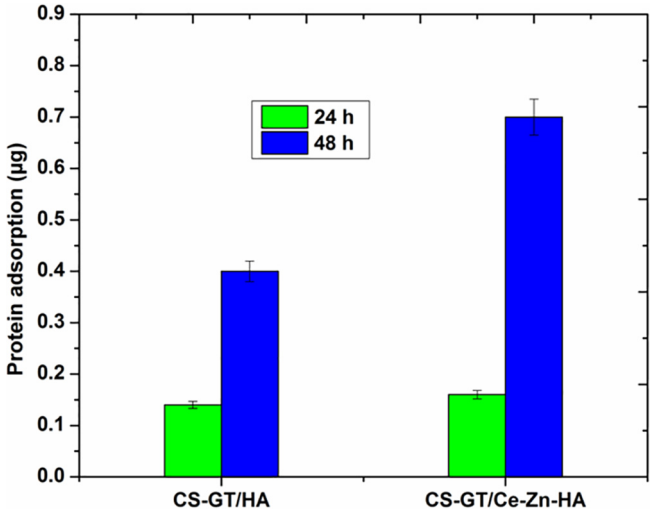

Fig. 4. Protein adsorption studies of prepared cryogel biocomposites.

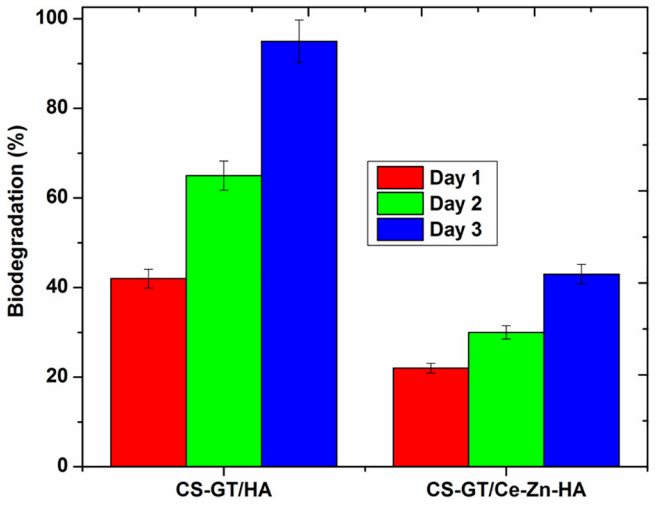

Fig. 3. Degradation studies of prepared cryogel biocomposites were carried out in the existence of lysozyme for 1 to 3 days at RT.

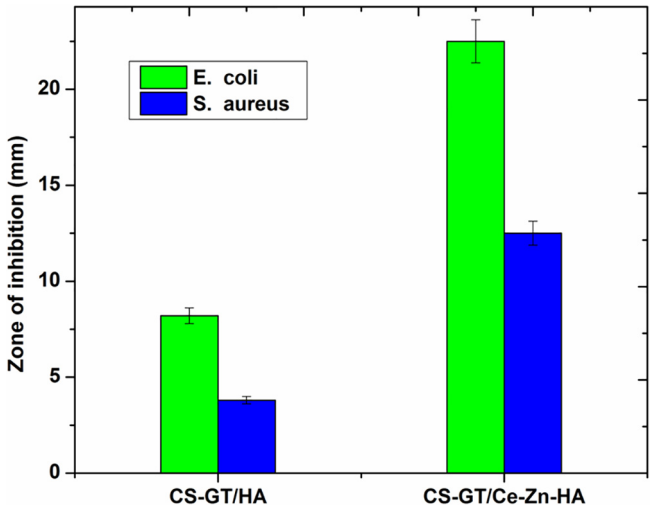

Fig. 5. Antibacterial activity of prepared cryogel biocomposites against *E. coli* and *S. aureus* bacteria.

It's noted that the antibacterial action of CS-GT/HA is because of the intrinsic bactericidal nature of CS. At the point when we recently arranged and decided HA doped Ce and Zn particles for bactericidal action, we found that HA went about as inactive material with no bactericidal movement (Gokcekaya et al., 2019). In this way, the expanded microbial zone of hindrance saw by the CS-GT/Ce-Zn-HA is because of the nearness of cerium–zinc particles.

3.6. Osteogenesis study

The capacity of CS-GT/Ce-Zn-HA cryogel biocomposite to improve osteogenic separation was assessed. The ALP actions of the cell-seeded on cryogel biocomposite were explored, and the outcome is introduced in Fig. 6a. Cells in the CS-GT/Ce-Zn-HA cryogel biocomposite showed an essentially higher ALP action contrasted with that on the CS-GT/HA layers following 1, 3 and 7 days of hatching, which infers that there was an advancement of osteogenic separation for cells in CS-GT/Ce-Zn-HA cryogel biocomposite.

To additionally consider the impacts of the CS-GT/Ce-Zn-HA cryogel biocomposite on osteogenic separation, mineralization of cells was seen by methods for ARS. As showed up in Fig. 6b, following 7 days of seeding, cells in CS-GT/Ce-Zn-HA cryogel biocomposite demonstrated increasingly clear positive recoloring of ARS than that on CS-GT/HA cryogel biocomposite. Also, the aftereffect of semi-quantitatively examination of Ca^{2+} content was as per the recoloring result referenced over, the outcomes showed that there was a striking contrast between cells refined in the CS-GT/Ce-Zn-HA composite platforms and on the CS-GT/-HA biocomposite films. These outcomes demonstrated that the CS-GT/Ce-Zn-HA cryogel

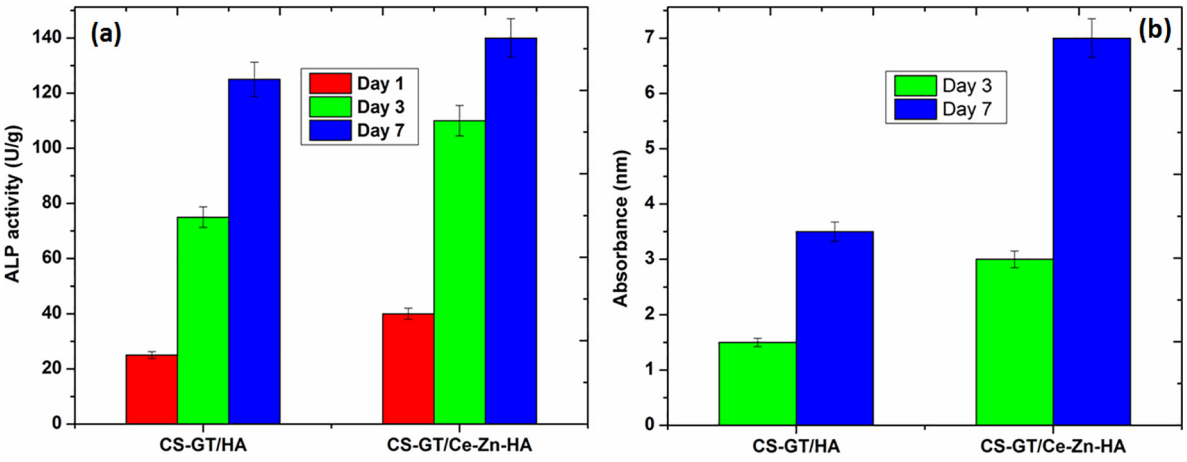

Fig. 6. (a) ALP activity and (b) Alizarin red S staining of cell-seeded on prepared cryogel biocomposites.

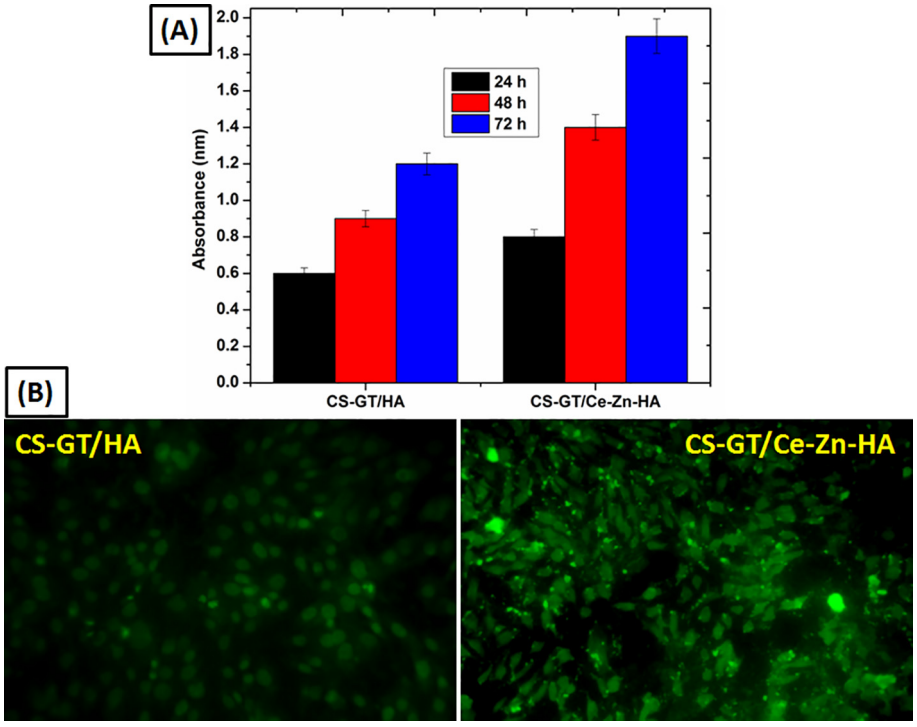

Fig. 7. (A) Proliferation of bone marrow stromal cells after 24, 48 and 72 h of culture on prepared samples. (B) Fluorescence images of bone marrow stromal cells after 3 days of culture prepared samples.

biocomposite encouraged the osteogenesis separation of cells contrasted with the CS-GT/HA cryogel biocomposite

All outcomes recommended that the novel CS-GT/Ce-Zn-HA cryogel biocomposite assumed a huge job in cell multiplication and separation, which showed a biomimetic microenvironment could control the osteogenic practices of cells. Also, the porous cryogel biocomposite can be custom fitted to various shapes and sizes satisfying the needs in the handy application. Along these lines, we unequivocally accepted that the CS-GT/Ce-Zn-HA cryogel biocomposite be potential up-and-comers in bone fixing and recovery later on.

3.7. Cytotoxicity and live/dead cell assay

To survey the impact of the permeable structure of CS-GT/Ce-Zn-HA cryogel biocomposite for the cell culture, the CCK-8 test was applied to assessed viability and multiplication. CS-GT/HA biocomposite layers were set as control. Cells were refined on frameworks and films for a time of 72 h As appeared in Fig. 7A, there is a comparative cell connection after 24 h of culture. Nonetheless, during the way of life of 24 h, 48 h and 72 h, cell multiplication of cells in CS-GT/Ce-Zn-HA cryogel biocomposite is fundamentally higher than that on the CS-GT/HA cryogel biocomposite. Contrasted with customary hydroxyapatite layers, these outcomes unmistakably demonstrated that the permeable spatial structure with high and profound interconnected pores of CS-GT/Ce-Zn-HA cryogel biocomposite could improve cell expansion.

Fig. 7B indicated CS-GT/HA and CS-GT/Ce-Zn-HA cryogel biocomposites incubated with bone marrow stromal cells in the wake of performing Live/Dead recoloring. From the fluorescence images, it could be seen that cells followed, multiplied, and stayed reasonable following 3 days incubation (Fig. 7B). The exceptionally low red fluorescence delineated in the pictures showed that there was a little figure of dead cells.

4. Conclusion

The fabricated CS-GT cryogel containing Ce-Zn-HA nanoparticles was described by XRD and SEM contemplates. The biocomposite uncovered the permeable engineering in the miniaturized scale extend proposed for cell entrance, bony tissue in development. These miniaturized scale and nano courses of action may be given an interface to all the more likely bone arrangement. The CS-GT/Ce-Zn-HA cryogel biocomposite had increased growth, diminished biodegradation, and expanded protein adsorption characteristics contrasted with CS-GT/HA cryogel biocomposite. The bactericidal and osteo-proliferative characteristics of the biocomposite were because of the nearness of Ce–Zn-HA nanoparticles and these properties would assist with limiting the implant-related bacterial contamination and to advance bone arrangement. Subsequently, this examination proposes that the CS-GT/Ce-Zn-HA cryogel biocomposite would be progressively useful for bone tissue designing applications.

Declaration of Competing Interest

The authors declare that they have no known competing financial interests or personal relationships that could have appeared to influence the work reported in this paper.

Acknowledgements

This work was supported by the Shandong Province Key Research and Development Program (No. 2016GGX103034).

References

Ansari, M., 2019. Bone tissue regeneration: biology, strategies and interface studies. Prog. Biomater., 1–15

Asadpour, S., Kargozar, S., Moradi, L., Ai, A., Nosrati, H., Ai, J., 2019. Natural biomacromolecule based composite scaffolds from silk fibroin, gelatin and chitosan toward tissue engineering applications. Int. J. Boil. Macromol.

Arcos, D., Vallet-Regí, M., 2020. Substituted hydroxyapatite coatings of bone implants. J. Mater. Chem. B 8, 1781–1800.

Anastasiou, A.D., Nerantzaki, M., Gounari, E., Duggal, M.S., Giannoudis, P.V., Jha, A., Bikiaris, D., 2019. Antibacterial properties and regenerative potential of Sr^{2+} and Ce^{3+} doped fluorapatites; a potential solution for peri-implantitis. Sci. Rep. 9, 1–11.

Bachmann, M., Kukkurainen, S., Hytönen, V.P., Wehrle-Haller, B., 2019. Cell adhesion by integrins. Physiol. Rev. 99, 1655–1699.

Carrabba, M., Madeddu, P., 2018. Current strategies for the manufacture of small size tissue engineering vascular grafts. Front. Bioeng. Biotechnol. 6, 41.

Dave, K., Gomes, V.G., 2019. Interactions at scaffold interfaces: effect of surface chemistry, structural attributes and bioaffinity. Mater. Sci. Eng. C, 110078.

Dasgupta, S., Banerjee, S.S., Bandyopadhyay, A., Bose, S., 2010. Zn-and Mg-doped hydroxyapatite nanoparticles for controlled release of protein. Langmuir 26, 4958–4964.

Gokcekaya, O., Ueda, K., Ogasawara, K., Narushima, T., 2019. Antibacterial activity of Ag nanoparticle-containing hydroxyapatite powders in simulated body fluids with Cl ions. Mater. Chem. Phys. 223, 473–478.

Hintermann, E., Christen, U., 2019. The many roles of cell adhesion molecules in hepatic fibrosis. Cells 8, 1503.

Huang, Y., Zhang, X., Mao, H., Li, T., Zhao, R., Yan, Y., Pang, X., 2015. Osteoblastic cell responses and antibacterial efficacy of Cu/Zn co-substituted hydroxyapatite coatings on pure titanium using electrodeposition method. RSC Adv. 5, 17076–17086.

Huang, C., Fang, G., Zhao, Y., Bhagia, S., Meng, X., Yong, Q., Ragauskas, A.J., 2019. Bio-inspired nanocomposite by layer-by-layer coating of chitosan/hyaluronic acid multilayers on a hard nanocellulose-hydroxyapatite matrix. Carbohydr. Polym. 222, 115036.

Kumar Meena, L., Rather, H., Kedaria, D., Vasita, R., 2020. Polymeric microgels for bone tissue engineering applications – a review. Int. J. Polym. Mater. Polym. Biomater. 69, 381–397.

Kumar, A., Kargozar, S., Baino, F., Han, S.S., 2019. Additive manufacturing methods for producing hydroxyapatite and hydroxyapatite-based composite scaffolds: a review. Front. Mater. 6, 313.

Kemençe, N., Bölgen, N., 2017. Gelatin-and hydroxyapatite-based cryogels for bone tissue engineering: synthesis, characterization, in vitro and in vivo biocompatibility. J. Tissue Eng. Regener. Med. 11, 20–33.

Liu, X., Ma, P.X., 2004. Polymeric scaffolds for bone tissue engineering. Ann. Biomed. Eng. 32, 477–486.

Liu, L., Yang, K., Li, S., Zhang, L., Zhang, Y., 2019. Poly (ether sulfone) nanoparticles and controllably modified nanoparticles obtained through temperature-dependent cryogelation. J. Appl. Polym. Sci. 136 (20), 47485.

Ma, Z.J., Yamaguchi, M., 2001. Role of endogenous zinc in the enhancement of bone protein synthesis associated with bone growth of newborn rats. J. Bone Miner. Metab. 19 (1), 38–44.

Milazzo, M., Contessi Negrini, N., Scialla, S., Marelli, B., Farè, S., Danti, S., Buehler, M. J., 2019. Additive manufacturing approaches for hydroxyapatite-reinforced composites. Adv. Funct. Mater. 29, 1903055.

Nikolova, M.P., Chavali, M.S., 2019. Recent advances in biomaterials for 3D scaffolds: a review. Bioact. Mater. 4, 271–292.

Ng, J., Spiller, K., Bernhard, J., Vunjak-Novakovic, G., 2017. Biomimetic approaches for bone tissue engineering. Tissue Eng. Part B: Rev. 23, 480–493.

Naganuma, T., Traversa, E., 2014. The effect of cerium valence states at cerium oxide nanoparticle surfaces on cell proliferation. Biomaterials 35, 4441–4453.

Parai, R., Bandyopadhyay-Ghosh, S., 2019. Engineered bio-nanocomposite magnesium scaffold for bone tissue regeneration. J. Mech. Behav. Biomed. Mater. 96, 45–52.

Phatai, P., Futalan, C.M., Utara, S., Khemthong, P., Kamonwannasit, S., 2018. Structural characterization of cerium-doped hydroxyapatite nanoparticles synthesized by an ultrasonic-assisted sol-gel technique. Results Phys. 10, 956–963.

Ren, F., Xin, R., Ge, X., Leng, Y., 2009. Characterization and structural analysis of zinc- substituted hydroxyapatites. Acta Biomater. 5, 3141–3149.

Saini, R.K., Bagri, L.P., Bajpai, A.K., 2019. Nano-silver hydroxyapatite based antibacterial 3D scaffolds of gelatin/alginate/poly (vinyl alcohol) for bone tissue engineering applications. Colloids Surf., B 177, 211–218.

Stevanović, M., Djošić, M., Janković, A., Rhee, K.Y., Mišković-Stanković, V., 2019. Electrophoretically deposited hydroxyapatite-based composite coatings loaded with silver and gentamicin as antibacterial agents-Review. J. Serb. Chem. Soc. 84, 1287–1304.

Tripathi, A., Melo, J.S., 2019. Cryostructurization of polymeric systems for developing macroporous cryogel as a foundational framework in bioengineering applications. J. Chem. Sci. 131, 92.

Yavarpanah, S., Seyfi, J., Davachi, S.M., Hejazi, I., Khonakdar, H.A., 2019. Evaluating the effect of hydroxyapatite nanoparticles on morphology, thermal stability and dynamic mechanical properties of multicomponent blend systems based on polylactic acid/Starch/Polycaprolactone. J. Vinyl Add. Tech. 25, E83–E90.

Yamaguchi, M., 2010. Role of nutritional zinc in the prevention of osteoporosis. Mol. Cell. Biochem. 338, 241–254.
Yang, F., Dong, W.J., He, F.M., Wang, X.X., Zhao, S.F., Yang, G.L., 2012. Osteoblast response to porous titanium surfaces coated with zinc-substituted hydroxyapatite. Oral Surg. Oral Med. Oral Pathol. Oral Radiol. 113, 313–318.
Yadav, T.C., Srivastava, A.K., Raghuwanshi, N., Kumar, N., Prasad, R., Pruthi, V., 2019. Wound healing potential of natural polymer: chitosan "A Wonder Molecule". Integrat. Green Chem. Sustain. Eng., 527–579
Zhu, L., Luo, D., Liu, Y., 2020. Effect of the nano/microscale structure of biomaterial scaffolds on bone regeneration. Int. J. Oral Sci. 12, 1–15.